Contributed paper

OPTO-ELECTRONICS REVIEW **12**(1), 139–148 (2004)

InGaAs for infrared photodetectors. Physics and technology

J. KANIEWSKI*[1] and J. PIOTROWSKI[2]

[1]Institute of Electron Technology, 32/46 Al. Lotnikow, 02-668 Warsaw, Poland
[2]Military Institute of Armament Technology, 7 Prymasa Wyszynskiego Str., 05-220 Zielonka, Poland

InGaAs is a variable band gap semiconductor with excellent transport and optical properties. This makes it attractive for electronic and optoelectronic devices. One of the most important applications is short wavelengh (1–3.6 μm) infrared photodetectors. Such devices are based on multilayer heterostructures with complex band gap and doping profiles. Significant progress in technology of the InGaAs heterostructures has been achieved with MBE and MOCVD growth. We discuss here the status and perspectives of infrared photodetectors based on advanced InGaAs heterostructures.

Keywords: InGaAs photodiodes, optical immersion, resonant cavity, Schottky photodiodes, avalanche photodiodes.

1. Introduction

The ternary variable gap semiconductor $In_xGa_{1-x}As$ is widely used for optoelectronic devices including infrared photodetectors. The devices could be optimised for any wavelength within a spectral range of 0.85–3.6 μm. The lattice parameter of $In_xGa_{1-x}As$ depends on a composition changing from a = 5.65 Å for GaAs (E_g = 1.435 eV) to a = 6.06 Å for InAs (E_g = 0.35 eV). With the exception of $In_{0.53}Ga_{0.47}As$ that is matched to InP, all other x materials grown on InP or GaAs are not lattice matched. $In_xGa_{1-x}As$ layers with sub-critical thickness can be easily defect free grown. Unfortunately, the growth of more thick layers is accompanied by generation of a dislocation and other defects. Efficient absorption of infrared radiation requires layers much thicker than the critical thickness value. Numerous measures have been developed to solve the problem including buffered and lateral growth.

Lattice mismatch presents also significant limitations on the growth of multiple layer heterostructures that are necessary for advanced photodetectors and other optoelectronic devices.

We discuss here physical aspects and practical problems of technology of $In_xGa_{1-x}As$ infrared photodetectors.

2. Conventional photodetectors

2.1. Fundamental limitations to performance of infrared $In_xGa_{1-x}As$ photodetectors

Detectivity D^* is the normalized detector signal-to-noise ratio that determines ability of the device to detect weak optical signals

$$D^* = \frac{R_i (A\Delta f)^{1/2}}{I_n}, \tag{1}$$

where R_i is the current responsivity, A is the optical area of a device, Δf is the bandwidth, and I_n is the noise current.

Detectivity is limited by the noise due to statistical nature of a generation-recombination (g-r) processes. When the thermal processes prevail, the ultimate D^* of the optimised device operating at near equilibrium conditions can be described as

$$D^* = 0.31 \frac{\lambda}{hc} \left(\frac{\alpha}{G} \right)^{1/2}, \tag{2}$$

where λ is the wavelength, h is the Planck constant, c is the light velocity, α is the absorption coefficient, and G is the thermal generation rate. There are fundamental and technological mechanisms of thermal generation and recombination. The technology related mechanisms (Shockley-Read, generation at surfaces and interfaces, tunnel generation and others) can be eliminated by progress in growth and processing.

Fundamental limits of $In_xGa_{1-x}As$ were discussed in Refs. 1, 2, and 3. Probably, the Auger A1, A7, and AS processes dominate in well-designed device. The role of radiative processes is less clear.

For Auger dominated device

$$D^* = 0.31 \frac{\lambda}{hc} \left(\frac{\gamma^{1/2} \tau_{A1}^i \alpha}{n_i} \right)^{1/2}, \tag{3}$$

where n_i is the intrinsic concentration, τ^i is the recombination time for A1, A7, and AS processes. The coefficient γ is

$$\gamma = \frac{\tau_{A7}^i \tau_A^i}{\tau_{A1}^i (\tau_{A7}^i + \tau_{AS}^i)}. \tag{4}$$

*e-mail: jkaniew@ite.waw.pl

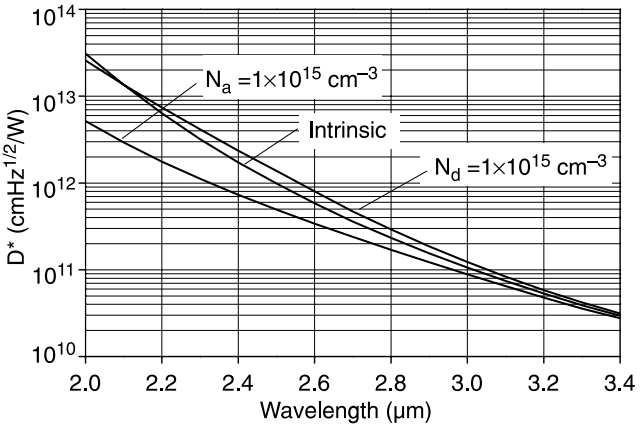

Fig. 1. Detectivity of $In_xGa_{1-x}As$ photodetectors as a function of the wavelength for which the detector is optimised.

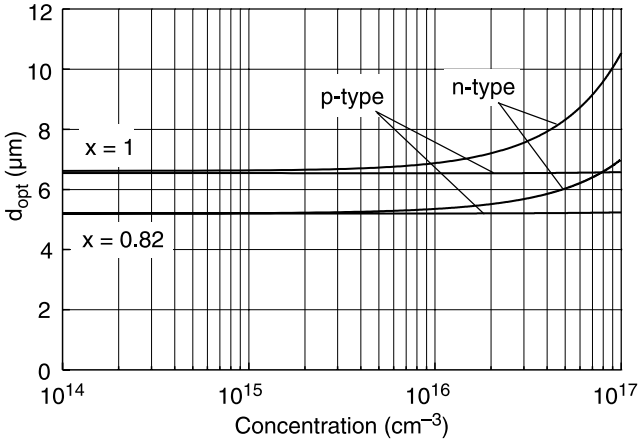

Fig. 3. Optimised absorber thickness for 2 μm ($x = 0.82$) and 3.4 μm ($x = 1$) devices. Single pass of radiation is assumed.

As shows Eq. (3), the ultimate detectivity significantly depends on the wavelength for which the detector is optimised. As calculated, the ultimate detectivity changes from 3×10^{13} cmHz$^{1/2}$/W for $\lambda = 2$ μm to 3×10^{10} cmHz$^{1/2}$/W for $\lambda = 3.4$ μm (Fig. 1).

The optimised $In_xGa_{1-x}As$ photodetectors require appropriate doping of the absorber region (Fig. 2). The doping level depends on the wavelength. The donor doping of 3×10^{15} cm^{-3} is suitable for >3 μm device while ≈ 1×10^{14} cm^{-3} for $\lambda = 2$ μm. So, pure material may be difficult to grow.

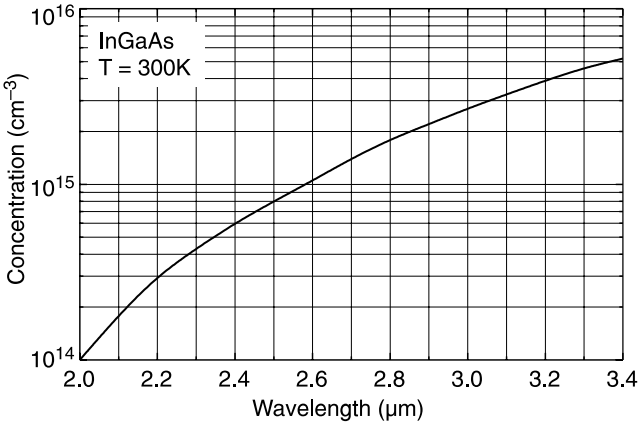

Fig. 2. Optimised doping level of $In_xGa_{1-x}As$ absorber as a function of the wavelength for which the detector is optimised.

Figure 3 shows an optimised thickness of an absorber. The thickness increases with a wavelength, changing from 5.2 μm to 6.7 μm for 2 μm and 3.4 μm wavelength for a single pass of IR radiation. It should be noted that double pass IR devices need absorbers thinner by a half. A thickness weakly depends on the absorber concentration (Fig. 3).

In addition to the absorber region, practical devices require additional regions that can sense charge carriers photogenerated in the absorber. The p^+-i-n^+ structure is typically used for a structure for $In_xGa_{1-x}As$ photovoltaic device. The performance of such devices can be affected by the additional thermal *g-r* processes at the p^+ and-n^+ regions, contacts, interfaces, space charge regions, and other noise sources. The common way to eliminate the detrimental processes is the use of sophisticated multilayer heterojunction device structures.

A frequency response of the photovoltaic devices is limited by a transport of the photogenerated charge carriers through the absorber region and by RC time constant. A transport through the absorber region is a combination of diffusion and drift. $In_xGa_{1-x}As$ is the material of choice for fast photodiode due to exceptionally large diffusion coefficient of electrons. It should be stressed that the frequency optimised $In_xGa_{1-x}As$ devices require lightly p-type doped absorber region for electron mobilities, much larger compared to that of holes.

The diffusion transport times at a room temperature are less than >100 ps for extrinsic p-type ≈ 5-μm thick InAs absorber. Further reduction can be achieved with the thinner absorber. Drift transport in reverse biased devices may reduce the transit time further.

The main limitation of response time typically comes from the RC time constant. For current mode operation, the RC time constant is determined by the junction capacitance and the photodiode series resistance. Reduction of series resistance by almost two orders of magnitude is possible using the structures with heavily doped n-type material for the mesa base, in comparison with p-type base of the same doping. This results in corresponding reduction of the RC time constant.

A very short RC time constant is expected in optically immersed photodiodes with a very small area of an active region. With these improvements, $In_xGa_{1-x}As$ photodiodes can be used for gigahertz range detection of IR radiation.

2.2. Optical immersion of infrared photodetectors

An efficient way to reduce the total thermal generation processes is reduction of physical size of the detector in comparison to its apparent optical size. Typically, this is

achieved by optical immersion of the detector to hemi- or hyperhemispherical lens prepared from a high refraction index material [4–6]. This can be implemented using monolithic optical immersion where the lens is formed in transparent detector substrate material.

Table 1 shows the gains due to use of GaAs immersion lens. This material with a large refraction index is transparent in a wide spectral range of (0.9–20 μm) and is frequently used as a substrate for device structures. As we can see, optical immersion significantly improves performance of IR devices.

Table 1. Relative gains due to use of optical immersion to GaAs lenses.

Parameter	Hemisphere		Hyper-hemisphere	
Linear size	n	(≈3.4)	n^2	(≈12)
Area	n^2	(≈12)	n^4	(≈134)
Voltage responsivity	n^2	(≈12)	n^4	(≈134)
Detectivity	n	(≈3.4)	n^2	(≈12)
Capacitance	n^2	(≈12)	n^4	(≈134)

Figures 4 and 5 show GaAs immersion lenses fabricated at the Vigo System S.A. using a monolithic approach. This technology requires relatively thick substrate, in dependence on a detector size. The lenses are prepared with numerically controlled mechano-chemical machinning.

Small immersion lenses (< 0.5 mm dia) and lens arrays are fabricated with photolithography-assisted micromachinning (Figs. 6 and 7).

2.3. Practical implementation of InAs/GaAs photovoltaic detector

The advanced InAs/GaAs photodetectors have been implemented by Institute of Electron Technology (ITE) in cooperation with VIGO SYSTEM S.A. The detector structures are grown by MBE at ITE while processing and lens fabri-

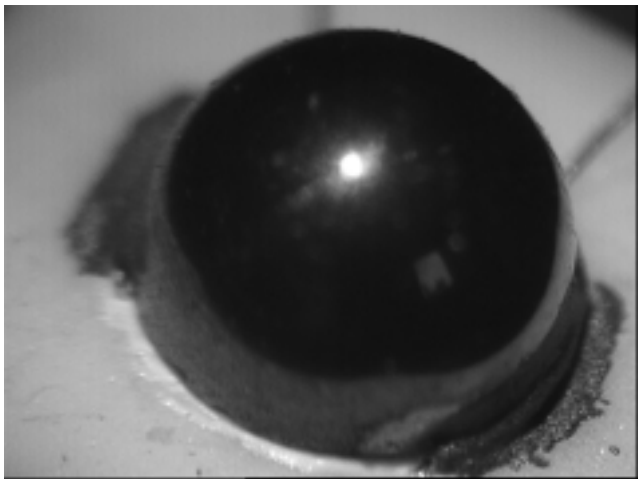

Fig. 4. 1-mm dia microlens prepared by mechano-chemical machining.

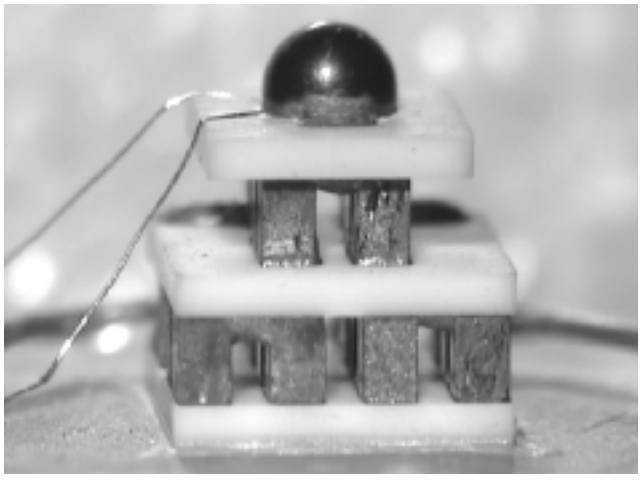

Fig. 5. Peltier cooled optically immersed In(GaAl)As photodetector.

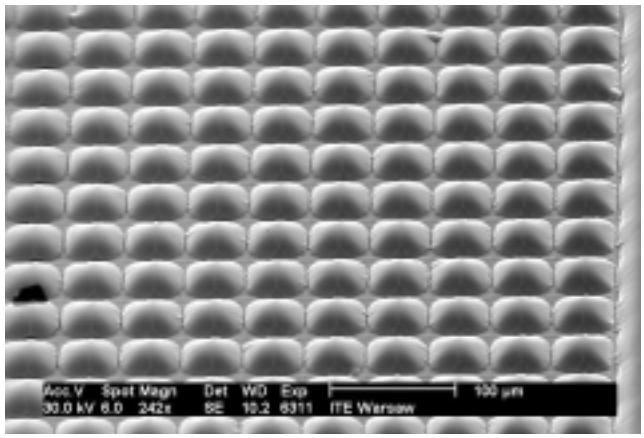

Fig. 6. Top view of a fragment of lens array with 50 μm pixel size.

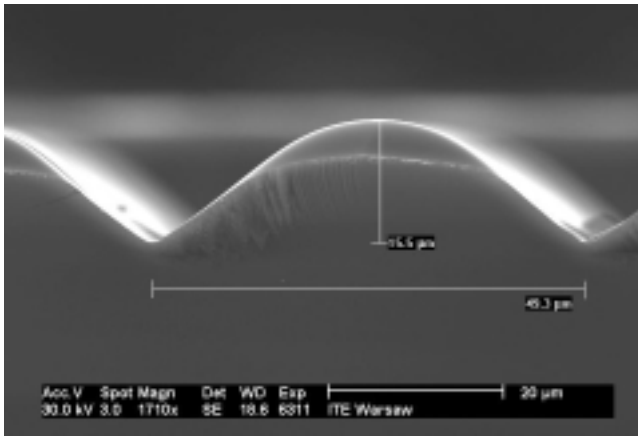

Fig. 7. SEM micrograph of 50 μm dia microlens. The lens shape approaches to some degree ideal spherical shape.

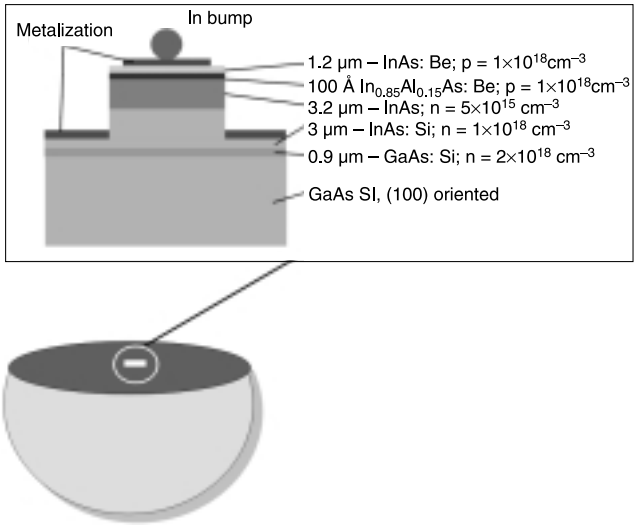

Fig. 8. InAs photovoltaic detector immersed to monolithic GaAs microlens.

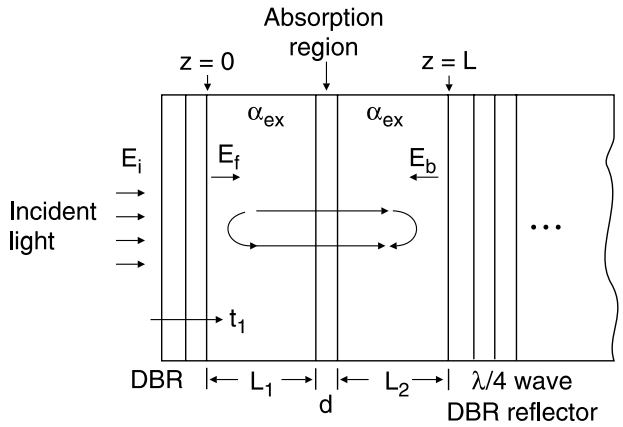

Fig. 9. Schematic representation of RCE detector (after Ref. 7).

cation is done at the VIGO SYSTEM SA. The devices are commercially available at present (www.vigo.com.pl).

The device employs backside illuminated $n^+nP^+p^+$ structure, schematically shown in Fig. 8. A metallic mirror at the top of a mesa structure ensures double pass of IR radiation, so relatively thin absorber can be applied. Heavily doped InAs n^+ layers are the mesa base, playing at the same time a role of the Burstain-Moss shifted window. A large thickness of the n^+ layer is used to reduce dislocation density in an absorber. Lightly doped InAs absorber ensures efficient operation up to $\lambda = 3.6$ μm. The strained P^+ wide gap InAlAs combined with the heavy doped p^+-InAs layer is used as the hole collector.

Such devices show detectivities of $\approx 7\times10^{10}$ cmHz$^{1/2}$/W at $T = 300$ K and 4×10^{11} cmHz$^{1/2}$/W with Peltier cooling ($T = 225$ K). This compares favourably, especially at a room temperature, with commercially available InAs devices. The quantum efficiency of 60% has been measured, slightly less than the reflection limit. It can be improved with a suitable AR coating.

The response time of the devices is less than 1 ns for the current mode zero bias conditions. 100 ps time constant has been observed for 0.2 V reverse bias in the optically immersed device of 1 mm^2 optical area. This is by two orders of magnitude better compared to non-immersed devices.

3. Resonant cavity enhanced photodetectors

3.1. Fundamental

In the resonant cavity enhanced photodetectors (RCE-PDs) both high bandwidth and high quantum efficiency can be achieved simultaneously due to multipass of infrared radiation that results in an efficient absorption in $<< 1/\alpha$ thick absorber.

The scheme of a generalized RCE-PD structure is presented in Fig. 9. The active region of the thickness d is a small gap semiconductor with the absorption coefficient α. It is positioned between the two mirror structures at the respective distances from the mirrors L_1 and L_2. The mirror can be formed by quarter-wave stack of large band gap semiconductors. The RCE-PD functions largely as a conventional device but is a subject to the effects of the cavity like wavelength selectivity and increase in the optical field. The quantum efficiency η for a RCE-PD structure with the lossless mirrors is [7,8]

$$\eta = \left[\frac{(1+R_2e^{-\alpha d})}{1-2\sqrt{R_1R_2}e^{-\alpha d}\cos(2\beta L+\psi_1+\psi_2)+R_1R_2e^{-\alpha d}}\right] \times (1-R_1)(1+e^{-\alpha d}), \quad (5)$$

where R_1 and R_2 are the top and bottom mirror reflectivities, respectively, ψ_1 and ψ_2 are the phase shifts introduced by the top and bottom mirrors and $L = L_1 + L_2 + d$.

Since the propagation constant β ($\beta = 2n\pi/\lambda_0$, where λ_0 is the vacuum wavelength and n is the refractive index) has wavelength dependence, η is the function of the wavelength as well. The calculated changes of wavelength dependency of a quantum efficiency are presented in Fig. 10. The curves correspond to $R_1 = 0.9$, 0.3, and 0.05 while $R_2 = 0.9$, $\alpha d = 0.1$ and $L = 2$ μm. The quantum efficiency η is enhanced periodically at a resonant wavelength when $2\beta L + \psi_1 + \psi_2 = 2\,m\pi$ ($m = 1, 2, 3$). The spacing of a resonant wavelength is defined as free spectral range FSR. The flat dotted line in Fig. 10 indicates the maximum η attainable for conventional photodetector for the same active layer thickness, $\alpha d = 0.1$. The contrast between two types of a detector is clear. Conventional detector operates at a broad-band while RCE detector can be designed for detection specific wavelength.

At the resonance wavelength [7,8]

$$\eta_p = \frac{1+R_2e^{-\alpha d}}{(1-\sqrt{R_1R_2}e^{-\alpha d})^2}(1-R_1)(1+e^{-\alpha d}). \quad (6)$$

From Eq. (6), the quantum efficiency at the certain αd value is maximised when

$$R_1 = R_2 e^{-2\alpha d}. \tag{7}$$

Figure 11 shows the maximum η_{max} as a function of αd for various R_2 values. To attain the highest η, near unity R_2 is desirable. For conventional detectors, without the cavity effect ($R_2 = 0$), quantum efficiency higher than 90% can be realized only for a thick (> 2 μm) active layer (curve $R_2 = 0$ in Fig. 11). For RCE detector, when $R_2 = 0.99$, the $\eta > 90\%$ can be obtained for < 0.05-μm thick layer ($\alpha = 10^4$ cm^{-1}). This fact is very helpful towards improving the high-speed performance of detectors reducing the electronic transit time.

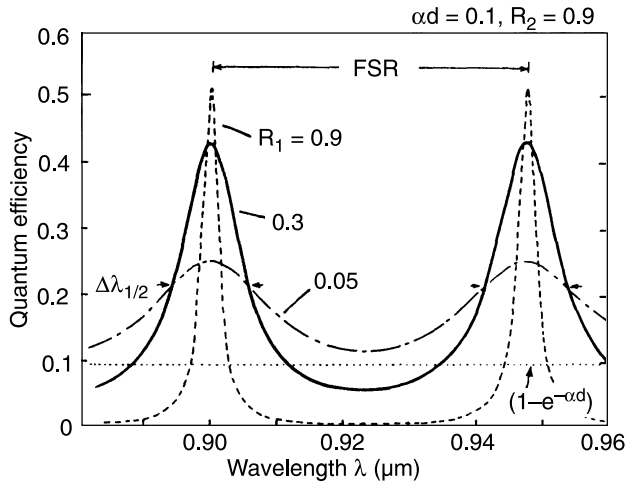

Fig. 10. Wavelength dependence of quantum efficiency for RCE detectors (after Ref. 7).

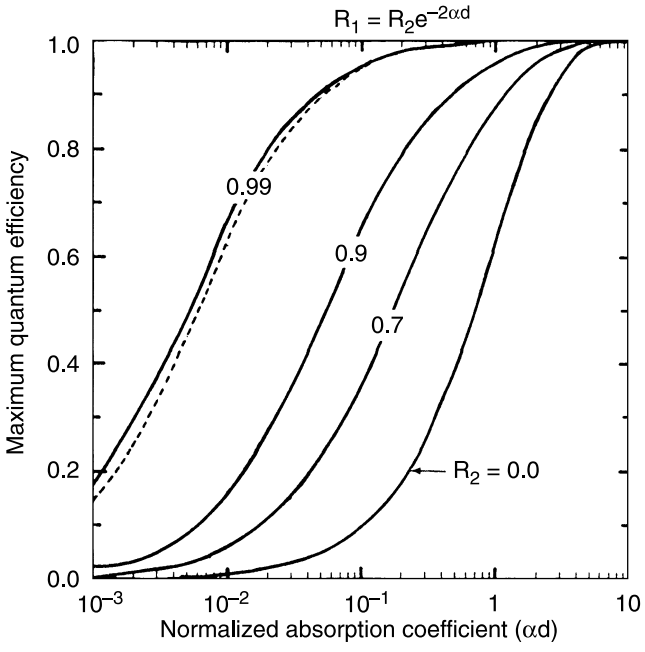

Fig. 11. Maximum quantum efficiency as a function of normalised absorption coefficient (after Ref. 7).

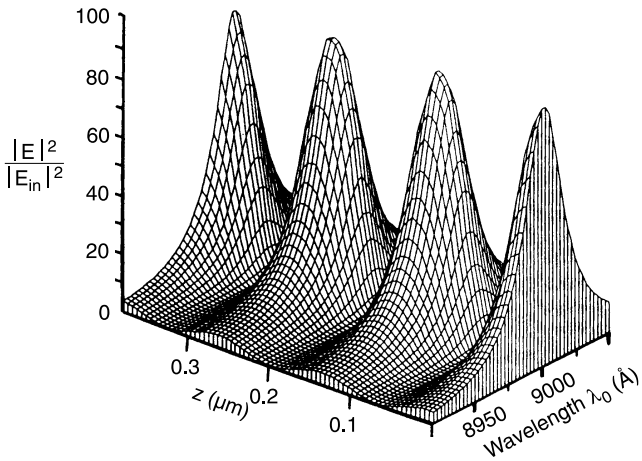

Fig. 12. Optical field distribution in RCE detector as a function of wavelength and position. Top and bottom mirrors are 5 and 15 periods GaAs/AlAs. Cavity is optimised for the wavelength of 0.9 μm (after Refs. 8 and 9).

The spatial distribution of the optical field inside the cavity is a specific feature of the cavity. It arises from the standing wave formed by the two propagating waves. A calculated distribution of the optical field is presented in Fig. 12. It follows that η, which is derived from the power absorbed in the active region, depends on a position of the active region in the optical field. In order to obtain maximum value of the detector efficiency, the active region should be placed in a wave antinode position.

The standing wave effect is conveniently included in the calculation of as an effective absorption coefficient, i.e., α_{eff} = SWE × α, where SWE is the standing wave coefficient. The SWE coefficient is an explicit function of the cavity properties [8,9].

Earlier, we confined our consideration of η to a normal incidence. The changes of a detector quantum efficiency versus angle incidence are presented in Fig. 13. The calcu-

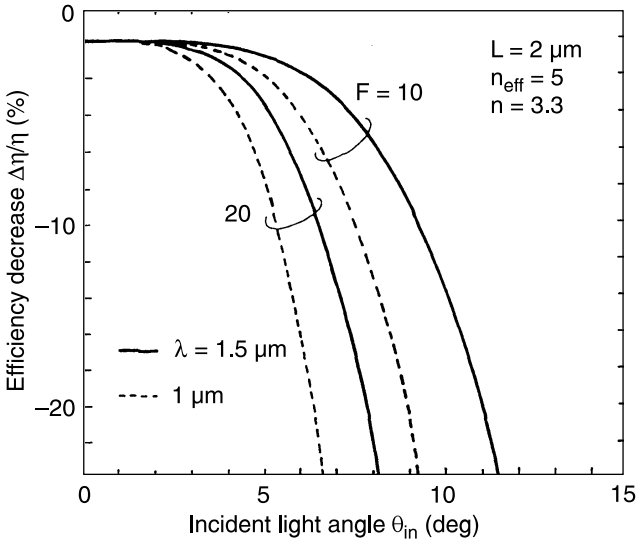

Fig. 13. Changes of η for off-angle incidence at λ = 1.0 μm and λ = 1.5 μm and different finesses F = 10 and F = 20 (after Ref. 7).

lations were performed for different wavelengths and different values of the finesse F (F = FSR/$\Delta\lambda_{1/2}$, where $\Delta\lambda_{1/2}$ is half width of a resonant peak). It indicates that η is the most sensitive to the angle of incidence in the high F cavity at the shorter λ and quantum efficiency degrades by 20% above 10°. The simulations show that RCE detectors cannot work well, even with quite slow optics.

The performance of RCE-PD mainly depends on the realization of a low loss cavity. The mirrors and cavity material must be non-absorbing at the detection wavelength and the mirrors must have high reflectivity. Generally, mirrors can be fabricated as metallic, dielectric, DBR (distributed Bragg reflectors made of semiconducting or dielectric layers) or hybride (DBR + metal).

The active layer material must have a smaller bandgap material than the mirror and cavity materials but it should not be so small that large heterojunction band offsets hinder the extraction of photogenerated carriers. The active layer absorption coefficient should be moderate, i.e., 10^3–10^4 cm^{-1} for the operation wavelength.

Different material combinations satisfy all of the above requirements. The InGaAs material system for RCE detection is used in two combinations of semiconductors, AlGaAs/GaAs/InGaAs and InP/InGaAs/InAlAs.

Application of InGaAs as the active material allows for extension device operation spectrum to the wavelength longer than 900 nm. This ternary compound containing small amount of In can be grown on GaAs substrate. In this case AlAs and GaAs, having good refractive index contrast, can be used for construction of the mirrors of the resonant cavity with nearly unit reflectivity with about twenty period quarter wave superlattice.

$In_xGa_{1-x}As$ containing higher amount of indium ($x \approx 0.5$) is usually grown on InP substrate. $In_{0.53}Ga_{0.47}As$ and $In_{0.52}Al_{0.48}As$ lattice matched to InP have rather poor refractive index contrast and increased number of periods (≈ 35) are required to achieve nearly unit reflectivity of the mirror. For the detectors operating at 1.3–1.55 μm wavelength range, quaternary compounds like InGaAlAs and InGaAsP lattice matched to InP are more suitable for mirror formation.

3.2. Practical implementation of RCE-PDs

To the date, InGaAs ternary compound has been the most commonly studied ternary compound for RCE detection because of the easiness with which GaAs and InP based heterostructures can be grown by molecular beam epitaxy (MBE) and metalorganic chemical vapour deposition (MOCVD) [10]. The capabilities have been demonstrated in many practical photodetectors.

3.2.1. RCE-Schottky photodetectors

The AlGaAs/GaAs/InGaAs based RCE-Schottky photodetector, presented in Ref. 11, operated at 895 nm.

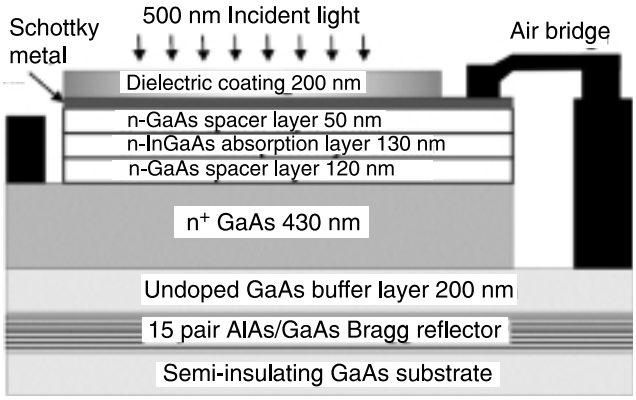

Fig. 14. Schematic cross-section of the RCE Schottky photodiode (after Ref. 11).

A schematic representation of this structure is shown in Fig. 14. The device structure was grown on a GaAs substrate by MBE. The cavity is formed by 15 pairs AlAs/GaAs DBR bottom reflector and a semi transparent Au contact on the top. The InGaAs absorption layer has an In mole fraction less than 10% and both heterojunctions are linearly graded for 25 nm to avoid carrier trapping. The position of the absorption layer in the depletion region is optimised to yield minimum transit time for electrons and holes [11]. The device was fabricated with mesa isolation. To reduce the parasitic capacitance of the photodetector, the Schottky metal was connected to the contact pads with an Au air-bridge. A 200 nm Si_3N_4 coating on the top was used.

The optimised RCE-Schottky photodiode has a 3 dB bandwidth of ≈100 GHz and bandwidth-efficiency product > 70 GHz.

Using the indium tin oxide (ITO) for the Schottky diode solves the problems of optical losses and scattering caused by the Schottky metal. For the RCE-ITO-Schottky diode fabricated by Biyikli *et al*. with an area of 5×5 μm, the bandwidth was 60 GHz while the quantum efficiency was 75% for a reverse voltage of 4 V [12]. This results in a bandwidth-efficiency product of 45 GHz.

3.2.2. RCE avalanche PD

The internal gain of avalanche photodiodes (APDs) provides substantial improvement in signal-to-noise characteristics compared to other types of PDs. The APD structure that has been widely deployed is the separate absorption and multiplication region (SAM) APD. It consists of a wide-bandgap multiplication region and a narrow-bandgap absorbing layer separated by a transition region that reduces the accumulation of a charge at the interface between the multiplication and absorption regions which improves the low-gain bandwidth.

In order to reduce the transit time and thus improve the frequency response at low gains, the APD layers are incorporated into a resonant-cavity structure [13,14]. The device

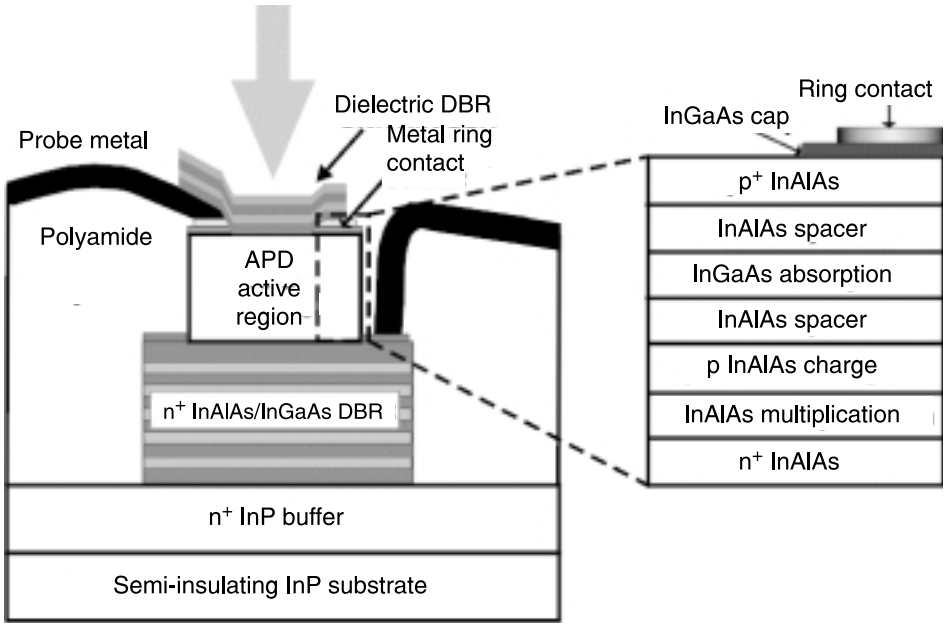

Fig. 15. Schematic cross-section of InGaAs-InAlAs SAM APD device (after Ref. 14).

structure is shown in Fig. 15. Starting from a semi-insulating InP substrate, the bottom mirror, which consisted of 30 $\lambda/4$ pairs of n^+-$In_{0.53}Ga_{0.47}As/In_{0.52}Al_{0.48}As$, was grown by MBE. After the growth of the thin undoped $In_{0.52}Al_{0.48}As$ multiplication region, a p-type $In_{0.52}Al_{0.48}As$ charge layer was inserted to ensure that the electric field in the adjacent absorption region would be $< 1\times10^5$ V/cm. This was followed by the 60 nm-thick $In_{0.53}Ga_{0.47}As$ absorption layer. Finally, an undoped $In_{0.52}Al_{0.48}As$ spacer and a p^+-$In_{0.52}Al_{0.48}As$ top layer were grown. To fabricate a high-speed device, first a Ti-Pt-Au contact metal ring was deposited and a mesa with the diameter of 14 μm was formed by chemical etching.

Due to the resonant-cavity scheme, these APDs operating at 1.55 μm exhibited high external quantum efficiency 70% and a high unity-gain bandwidth of 24 GHz. Utilizing the excellent noise characteristics of a thin InAlAs multiplication region, a record value of a gain-bandwidth product of 290 GHz was achieved.

3.2.3. RCE p-i-n PD

The first RCE p-i-n was reported by Dentai *et al*. who studied an InGaAs/InGaAsP/InP structure designed to operate near 1.55 μm [15]. A quantum efficiency of 82% was achieved using a 200 Å InGaAs absorbing layer with R_1 = 0.7 and R_2 = 0.95.

RCE p-i-n PDs with a periodic absorber structure were demonstrated by Huang *et al*. to detect 870-nm wavelength [16]. Figure 16(a) depicts the schematic structure of a typical RC photodiode with a single absorbing layer placed in a wave antinode position. In order to improve quantum efficiency of RCE p-i-n PD, it was proposed to use a triple layer as the active medium. The thickness of the spacer layers were chosen so that the three absorbing layers are located at the antinodes of the standing wave optical field in the cavity [Fig. 16(b)]. The investigated devices, shown schematically in Fig. 17(a), were grown by MBE on n^+-GaAs substrate. Thirteen period AlAs/GaAs quarter-wave stacks formed bottom mirror with the reflectivity about 90% at the centre wavelength 900 nm. The three $In_{0.05}Ga_{0.95}As$ active layers with each layer of the thickness 40 nm were sandwitched between GaAs layers. The top mirror with 30% reflectivity was formed by air and semiconductor interface.

The peak quantum efficiency of the triple-layer resonant-periodic-absorber photodiode was 65% [see Fig. 17(b)]. An enhancement of 30% has been achieved by a periodic absorber structure as compared to a standard RCE photodiode with a single absorbing layer of the same total thickness.

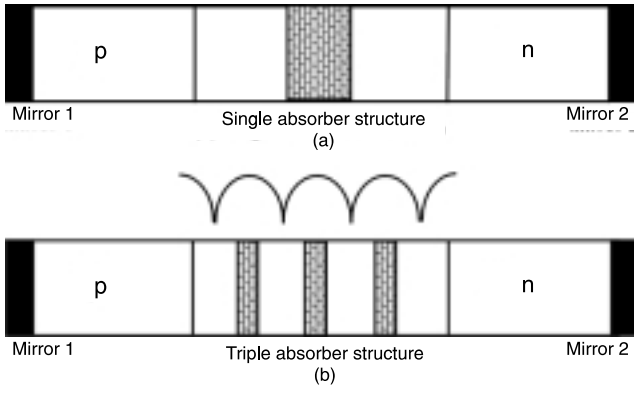

Fig. 16. Schematic structures of RCE PD with a single absorbing layer (a) and resonant-periodic-absorber RCE PD with triple layers as the absorbing medium (b) (after Ref. 16).

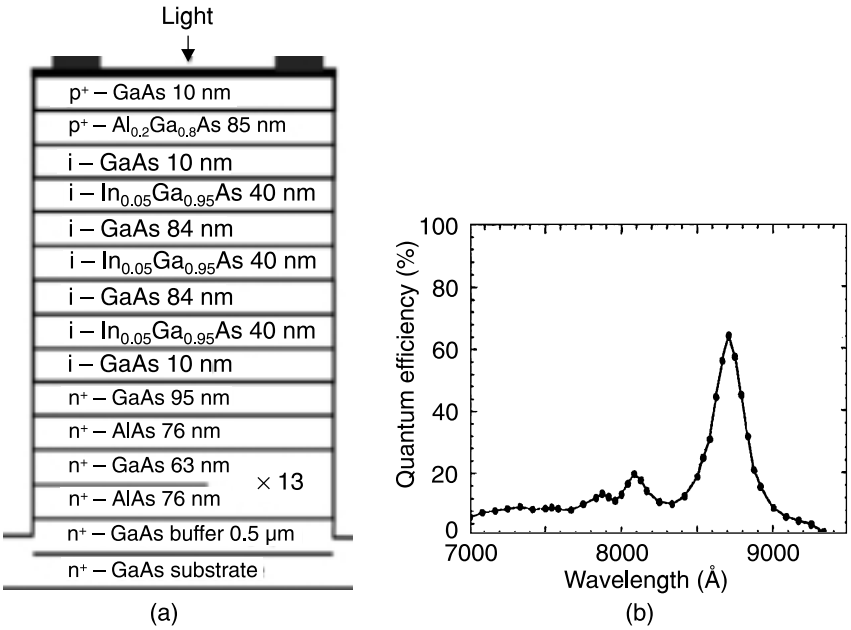

Fig. 17. Schematic structure of InGaAs resonant-periodic-absorber RCE PD (a), quantum efficiency of the structure (b) (after Ref. 16).

In order to simplify InGaAs/InP RCE p-i-n PD structure different types of reflectors can be used. Schematic structure of the RCE device utilizing hybrid reflector and semiconducting DBR is presented in Table 2.

The device is illuminated from the bottom. A detector is grown on SI-InP substrate. The bottom DBR is made of $In_{0.52}Al_{0.48}As$ and $In_{0.53}Ga_{0.32}Al_{0.15}As$ alternative layers. The resonant cavity is formed by 78 nm thick $In_{0.53}Ga_{0.47}As$ absorption layer, two $In_{0.52}Al_{0.48}As$ spacer layers together with two contact $In_{0.52}Al_{0.48}As$ layers. Top mirror consists of the dielectric DBR and Al layer. The detector structure was optimised using transfer matrix method. The calculations were performed for the device structure operating at $\lambda = 1548$ nm. The changes of absorption of 78-nm thick active layer versus amount of $In_{0.52}Al_{0.48}As/In_{0.53}Ga_{0.32}Al_{0.15}As$ pairs (bottom reflector) and Si_3N_4/SiO_2 pairs in top reflector are presented in Fig. 18. It has been found that more than 90% absorption of the active layer is obtained when 9 pairs in bottom reflector and 3 pairs in top reflector are used (Fig. 19).

This result is very important, because relatively small number of pairs is required for mirror formation. Additionally, very thin active layer results in subpicosecond transit time of the RCE p-i-n PD. High quantum efficiency for a narrow absorption line centred at 1548 nm can be obtained. The structure can be easily fabricated by MBE.

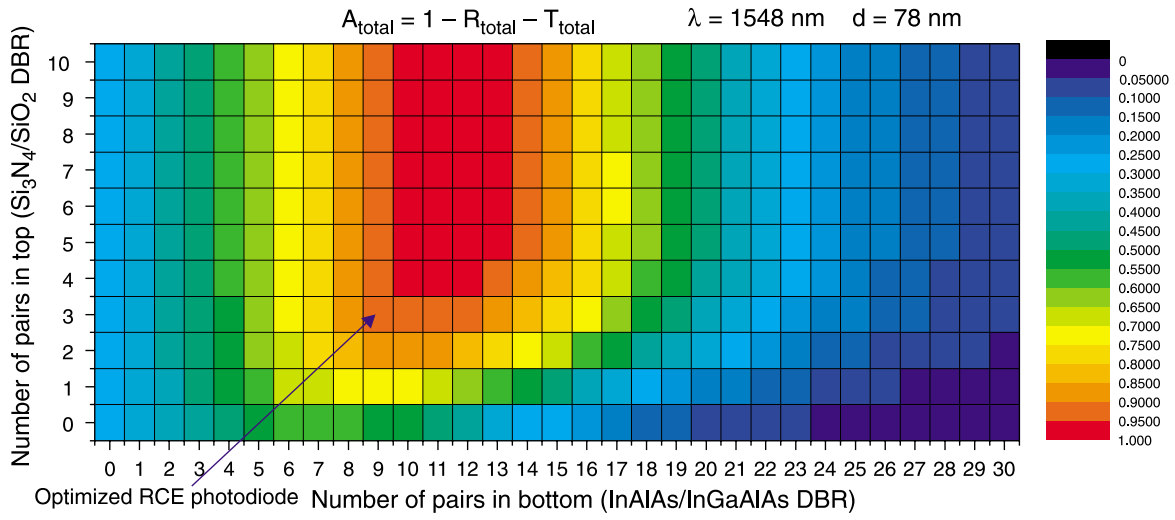

Fig. 18. Absorption of 78 nm thick $In_{0.53}Ga_{0.47}As$ active layer of RCE p-i-n PD for different numbers of pairs of layers in bottom and top reflectors.

Table 2. Structure of InGaAs RCE p-i-n PD grown onto InP.

Hybrid reflector-top	Metallic layer	Al
	Dielectric DBR	Si_3N_4/SiO_2
Cavity	Contact layer	p^+ $In_{0.52}Al_{0.48}As$
	Spacer layer	n^- $In_{0.52}Al_{0.48}As$
	Absorption layer	n^- $In_{0.53}Ga_{0.47}As$
	Spacer layer	n^- $In_{0.52}Al_{0.48}As$
	Contact layer	n^+ $In_{0.52}Al_{0.48}As$
Semiconducting reflector-bottom	DBR -bottom	$In_{0.52}Al_{0.48}As$/ $In_{0.53}Ga_{0.32}Al_{0.15}As$
	Substrate	SI-InP
	Antireflection coating	Si_3N_4

4. Conclusions

InGaAs ternary compound is widely used for detection of short wavelenth infrared radiation. Modern InGaAs detectors are fabricated by means of MBE and MOCVD technologies and advanced processing. It allows for production of discrete photodiodes, arrays, as well as optical integrated devices.

Conventional detectors can operate at a wide spectral range whereas RCE PDs are capable to detect narrow resonant wavelength only. The increased optical field allows RCE PD to be thinner and therefore faster than conventional one. RCE PDs exhibit high bandwidth and high external quantum efficiency as well.

The refractive microlenses can be used as optical concentrators for conventional photodetectors. They allow for improvement in performance and speed of response of devices. In the case of RCE PDs, strong degradation of quantum efficiency for off-normal angle incident radiation is observed.

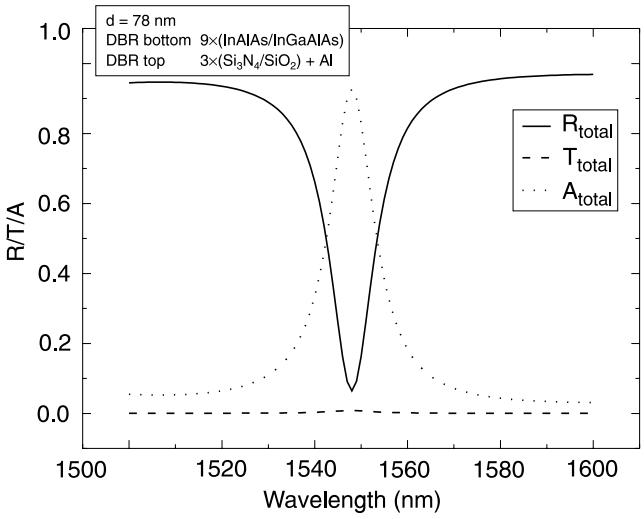

Fig. 19. Spectral dependence of: absorption A_{total} – dotted line, reflection R_{total} – solid line, and transmission T_{total} – dashed line, 78 nm thick $In_{0.53}Ga_{0.47}As$ active layer of optimised RCE p-i-n PD.

Acknowledgements

The authors would like to thank Dr Jan Muszalski for modelling and optimisation of InGaAs/InP RCE photodiodes. This work was partially supported by the Polish Committee for Scientific Research under grant No. 4 T11B 015 25.

References

1. J. Piotrowski and J. Kaniewski, "Optimisation of InGaAs infrared photovoltaic detectors", *IEE Proc. Optolectron.* **146**, 173–176 (1999).
2. J. Piotrowski, J. Kaniewski, and K. Reginski, "Modelling and optimisation of InGaAs infrared photovoltaic detectors", *Nucl. Instr. Methods in Phys. Res.* **A439**, 647–650 (2000).
3. A. Rogalski, "Performance limitations of InGaAs photodiodes", *Proc. SPIE* **3725**, 260–269 (1999).
4. E.L. Dereniak and G.D. Boreman, *Infrared Detectors and Systems*, J. Wiley and Sons, N.Y., 1996.
5. R.C. Jones, "Immersed radiation detectors", *Appl. Optics* **5**, 607–613 (1962).
6. J. Kaniewski, Z. Orman, J. Piotrowski, K. Reginski, and M. Romanis, "Advanced InGaAs detectors on GaAs substrates", *Proc. SPIE* **4130**, 749–759 (2000).
7. K. Kishino, M.S. Unlu, J. Chyi, J. Reed, L. Arsenault, and H. Morkoc, "Resonant cavity-enhanced (RCE) photodetectors", *IEEE J. Quantum Electron.* **27**, 2025–2034 (1991).
8. M.S. Unlu and S. Strite, "Resonant cavity enhanced photonic devices", *J. Appl. Phys.* **78**, 607–639 (1995).
9. M.S. Unlu, K. Kishino, H.J. Liaw, and H. Morkoc, "A theoretical study of resonant cavity-enhanced photodetectors with Ge and Si active regions", *J. Appl. Phys.* **71**, 4049–4058 (1992).
10. Y.M. El-Batawy and M.J. Deen, "Resonant cavity enhanced photodetectors (RCE-PDs): structure, material, analysis and optimisation", *Proc. SPIE* **4999**, 363–378 (2003).
11. B.M. Onat, M. Gokkavas, E. Ozbay, E.P. Ata, E. Towe and M.S. Unlu, "100-GHz resonant cavity enhanced Schottky photodiodes", *IEEE Photon. Technol. Lett.* **10**, 707–709 (1998).
12. N. Biyikli, I. Kimukin, O. Aytur, M. Gokkavas, M.S. Unlu, and E. Ozbay, "45 GHz bandwith-efficiency resonant-cavity enhanced ITO-Schottky photodiodes", *IEEE Photon. Technol Lett* **13**, 705–707 (2001).
13. S.S. Martuza, K.A. Anselm, C. Hu, H. Nie, B.G. Streetman, and J.C. Campbell, "Resonant cavity enhanced (RCE) separate absorption and multiplication (SAM) avalanche photodetector (APD)", *IEEE Photon. Technol. Lett.* **7**, 1486–1488 (1995).
14. C. Lenox, H. Nie, P. Yuan, G. Kinsey, A.L. Holmes, G.B. Streetman, and J.C. Campbell, "Resonant cavity InGaAs-InAlAs avalanche photodiodes with gain-bandwidth product of 290 GHz", *IEEE Photon. Technol. Lett.* **11**, 1162–1164 (1999).

15. A.G. Dentai, R. Kuchibhotla, J.C. Campbell, C. Tsai, and C. Lei, "High quantum efficiency long-wavelength InP/InGaAs microcavity photodiode", *Electron. Lett* **27**, 2125–2127 (1991).

16. F.Y. Huang, A. Salvador, X. Gui, N. Teraguchi, and H. Morkoc, "Resonant-cavity GaAs/InGaAs/AlAs photodiodes with a periodic absorber structure", *Appl. Phys. Lett.* **63**, 141–143 (1993).

